

# 1 Performance of GPCP Products Over Oceans: 2 Evaluation Using Passive Aquatic Listeners

3 **Zhe Li<sup>1</sup>, Elizabeth J. Thompson<sup>2</sup>, Ali Behrang<sup>3</sup>, Haonan Chen<sup>1</sup>, Jie Yang<sup>4</sup>**

4 <sup>1</sup>Department of Electrical and Computer Engineering, Colorado State University, Fort Collins, CO 80523,  
5 USA

6 <sup>2</sup>NOAA Physical Sciences Laboratory, Boulder, CO 80305, USA

7 <sup>3</sup>Department of Hydrology and Atmospheric Sciences, The University of Arizona, Tucson, AZ 85721, USA  
8 <sup>4</sup>Applied Physics Laboratory, University of Washington, Seattle, WA 98105, USA

## 9 **Key Points:**

- 10 • Passive Aquatic Listeners (PALs) are used to validate GPCP products over global  
11 oceans.
- 12 • Newly released GPCP Version 3.2 and the previous Version 1.3 daily products are  
13 compared.
- 14 • The performance of GPCP products depends on time scale, location, and rain-  
15 fall intensity.

---

Corresponding author: Dr. Zhe Li, [zhe.li@colostate.edu](mailto:zhe.li@colostate.edu)

16      **Abstract**

17      Passive Aquatic Listeners (PALs) have been increasingly deployed to collect minute-scale  
 18      surface oceanic rainfall and wind information, with a sampling area similar to the space-  
 19      borne sensor footprints. This provides an unprecedented opportunity to validate satel-  
 20      lite precipitation products over oceans. This study evaluates the Global Precipitation  
 21      Climatology Project (GPCP) daily products, including the widely-used GPCP v1.3 and  
 22      the newly released GPCP v3.2, over oceans using 58 PALs as references. The study shows  
 23      that the GPCP performance depends on time scale, region, and rainfall intensity. The  
 24      two versions of GPCP perform similarly at multi-year and monthly scales, while GPCP  
 25      v3.2 shows substantial improvements in representing rain occurrence and rain intensity  
 26      at daily scale. The results also highlight the challenge of precipitation measurement over  
 27      certain regions such as the tropical Northeastern Pacific and extratropical North Pacific,  
 28      where both versions of the GPCP products perform similarly but exhibit noticeable dif-  
 29      ferences compared to PAL observations.

30      **Plain Language Summary**

31      Satellites are the main instruments to quantify precipitation over the ocean, but  
 32      it is difficult to check their accuracy because we do not have many rain gauges over oceans  
 33      to compare with satellites. The Passive Aquatic Listener (PAL) is “the underwater phone”  
 34      to listen to the sound generated when raindrops hit the sea surface. The PAL estimates  
 35      rain rates based on the loudness of the sound at each frequency. This is similar to lis-  
 36      tening to the rain under a tin roof. PAL can drift with ocean currents for years, so it can  
 37      collect rainfall data over a large ocean area. The Global Precipitation Climatology Project  
 38      (GPCP) product is a popular long-term satellite-based precipitation data record to study  
 39      climate, water cycle, and the ocean. This study uses PAL observations to evaluate the  
 40      performance of GPCP’s latest two versions: v1.3, and the newly released GPCP v3.2.  
 41      The results show that the new product is better than the old product in estimating daily  
 42      rainfall, while they are similar when estimating monthly and multi-year rainfall. We also  
 43      notice that they provide similar estimates, which are both quite different from PAL ob-  
 44      servations, over the tropical Northeastern Pacific and extratropical North Pacific.

45      **1 Introduction**

46      Precipitation is an essential component of the global water and energy cycles. For  
 47      this reason, it has long been recognized that accurate knowledge of the time, amount,  
 48      and distribution of precipitation plays a fundamental role in understanding the Earth’s  
 49      climate system (Hartmann, 2016). As the largest reservoir of water in this system, the  
 50      oceans receive over 75% of global precipitation and contribute approximately 85% of at-  
 51      mospheric water vapor through evaporation (Lagerloef et al., 2010). The difference be-  
 52      tween precipitation and evaporation (also known as the ocean-atmosphere freshwater flux)  
 53      directly affects the upper ocean temperature, salinity, density, stability, and turbulence  
 54      (Moum & Smyth, 2019; Sallée et al., 2021; O’Kane et al., 2016). This influences oceanic  
 55      and atmospheric circulations and heat content, which regulate climate variability across  
 56      multiple scales (Schmitt, 1995; Durack, 2015). Despite its importance, oceanic precip-  
 57      itation remains one of the least understood elements in the Earth’s climate system due  
 58      to the lack of in-situ observations over oceans (Trenberth et al., 2007; Kidd et al., 2017).

59      To fill this gap, satellites have played a major role to quantify oceanic precipita-  
 60      tion. The precipitation-capable spaceborne sensors include infrared (IR), passive microwave  
 61      (PMW) imagers/sounders, and radars. Since each type of sensor has its own strengths  
 62      and limitations, today’s satellite-based precipitation products are built upon a multi-sensor  
 63      approach, which integrates the measurements from a constellation of spaceborne sensors  
 64      to maximize the accuracy, coverage, and resolution of precipitation estimates on a global  
 65      scale (Kidd et al., 2021). Furthermore, long-term climate records of global precipitation

can only be achieved through such a multi-sensor strategy (Levizzani et al., 2018). In this regard, the Global Precipitation Climatology Project (GPCP) was developed by merging PMW/IR sensors and rain gauges (over land) to provide this information to the international community. For a long time, GPCP linked to the World Climate Research Programme (WCRP) and Global Energy and Water Experiment (GEWEX) activities (Adler et al., 2020).

GPCP was first introduced in the mid-1990s (Arkin & Xie, 1994; Huffman et al., 1997), and since then, it has undergone several iterations to improve the input data sources, merging algorithms, and resolution (Huffman et al., 2001; Adler et al., 2003; Huffman et al., 2023a). GPCP products have been widely used to study the precipitation climatology and the hydrologic cycle (e.g., Yu, 2011; Lagerloef et al., 2010). However, validating satellite-based precipitation estimates, including GPCP, over oceans remains challenging. The in-situ reference data for validation are generally limited to rain gauges, which are only available from a small number of atoll/islands sites, moored buoys, and research vessels (Bowman, 2005; Sapiano & Arkin, 2009; Pfeifroth et al., 2013; Bolvin et al., 2021). Additionally, rain gauges may provide an incomplete representation of precipitation compared to satellite data, due to the point sampling nature of gauges relative to satellite grid box estimates that are several kilometers wide (Kidd et al., 2021). To overcome data limitations at sea, several other ocean-specific precipitation instruments have emerged, such as ship-based optical disdrometers (Klepp et al., 2018), ship-based motion-stabilized radars (Rutledge et al., 2019), and the subsurface Passive Aquatic Listeners (PAL; Ma & Nystuen, 2005; Yang et al., 2015).

Different from rain gauge or ship-based sensors, PAL is an underwater acoustic sensor (hydrophone) typically mounted on drifting Argo floats (Roemmich et al., 2019), which can collect oceanic rainfall and wind information at minute-scale over a large domain. In addition, a PAL has a sampling area similar to the footprint of spaceborne sensors, making it more comparable to satellite data. Since 2010, 58 PALs have been deployed over different oceans, and their observations were recently reprocessed and made available for use (Yang et al., 2015; Bytheway et al., 2023). In this study, we leverage this newly-available oceanic rainfall dataset to validate GPCP daily products over the ocean. To our best knowledge, this work represents the most expansive validation of GPCP daily data over oceans because it uses the distributed set of in-situ observations available from the state-of-the-art multiyear PAL database.

## 2 Data

### 2.1 Passive Aquatic Listeners

PAL is an innovative acoustic sensor, a hydrophone, designed to measure rain rate and wind speed routinely over the ocean (J. A. Nystuen et al., 2015; Yang et al., 2015). It collects underwater ambient-noise time series at different frequencies and converts them into a multi-frequency (1-50 kHz) spectrum of sound pressure levels (SPL). The overall SPL can be attributed to different sources of ocean ambient sound such as raindrops, surface wind, wave breaking, marine mammals, and ship traffic. Each of these sound sources has a unique spectral shape in terms of its SPL-frequency relation (for more details, see Yang et al., 2015; Ma, 2022). These relationships help determine the dominant ambient-noise source for each SPL spectrum, and, in the case of rainfall and surface wind speed, its intensity. Once the SPL spectrum is classified as either dominated by rain or wind, the SPL data at specific frequencies are used to estimate rain rate and wind speed, respectively. For example, if it is classified as rain, the SPL at 5 kHz ( $SPL_5$ ; in dB) is used to estimate rain rate ( $RR$ ;  $\text{mm h}^{-1}$ ) using a calibrated  $SPL_5$ - $RR$  relationship. PAL-measured acoustic intensity correlates with rain rate, from light to heavy rainfall (Yang et al., 2023). PAL is capable of reliably detecting rain rate of 0.2 mm/hour and has recorded rainfall rates up to 180 mm/hour over the Eastern Tropical Pacific. The sound of drizzle and

117 light rain is actually the most distinctive, so the PAL algorithm performs incredibly well  
 118 at the lowest rain rates. At wind speeds greater than about 15 m/s, bubbles entrained  
 119 into the ocean from breaking waves attenuate sound from raindrops hitting the ocean  
 120 surface, so quantitative rain retrievals become impossible beyond this wind speed.

121 Since 2010, 58 PALs (3 on moorings and 55 on Argo floats) have been deployed during  
 122 different field campaigns, in which the reliability of PAL-measured rain rates and wind  
 123 speeds has been verified against other in-situ measurements from the field campaigns (Ma  
 124 & Nystuen, 2005; Riser et al., 2019). In general, the uncertainty of PAL-measured rainfall  
 125 is about 10% (Yang et al., 2015), which is similar to the uncertainty level of other  
 126 in-situ rainfall measurements given the log-normal behavior of rain rate distributions.

127 PALs have been mounted on drifting Argo floats and stationary mooring buoys to  
 128 support recent ocean field campaigns, including NASA's Aquarius Mission (J. Nystuen  
 129 et al., 2011), Salinity Processes in the Upper Ocean Regional Study campaigns (SPURS-  
 130 1 and SPURS-2, E. Lindstrom et al., 2015; E. J. Lindstrom et al., 2019), and NOAA's  
 131 Tropical Pacific Observing System (TPOS, Smith et al., 2019). The PAL collects data  
 132 along the drifting trajectory of the Argo float. Typically, the Argo float drifts at 1-km  
 133 depth for approximately 9.5 days between the vertical profiling and surface communica-  
 134 tion cycles, and the attached PAL records rain rate data at 2-9 minute sampling in-  
 135 tervals when rainfall is detected (otherwise, wind speed is recorded). The Argo float typ-  
 136 ically traverses less than 3 km/day at this depth. PAL has a circular listening area ap-  
 137 proximately 5 km in diameter when drifting at 1-km depth, making it comparable to space-  
 138 borne sensors as they have similar sampling footprint sizes (Yang et al., 2015; Bytheway  
 139 et al., 2023). PALs on moorings have been deployed at variable depths (e.g., 1 km or a  
 140 few hundred meters). Their surface sampling diameter is smaller, at scales as about 5  
 141 × the depth.

142 Figure 1 shows the trajectories or locations of 58 PALs in the current database, span-  
 143 ning the Pacific, North Atlantic, and tropical Indian Oceans. These PALs were deployed  
 144 at different times (between 2010 and 2020) and their operational period varies (1-4 years),  
 145 so the number of PALs available at any given time and location is highly variable. The  
 146 rain rate and wind speed observations from these PALs were recently reprocessed into  
 147 regular 1-minute intervals and made available for use (Bytheway et al., 2023). The dataset  
 148 archive can be accessed through NASA EARTHDATA portal (the URL is provided in  
 149 the Open Research Section), and more details of PALs (e.g., the ID, operational period,  
 150 drifting extent) can be found in the Supporting Information.

## 151 2.2 GPCP Daily Precipitation Products

152 The GPCP Version 1.3 (hereinafter referred to as "GPCP v1.3") is the first-generation  
 153 GPCP daily product to provide 1° gridded precipitation estimates over the entire globe  
 154 from October 1996 to present (Adler et al., 2017). It is based on the One-Degree Daily  
 155 (1DD) technique, which was detailed in Huffman et al. (2001). This technique consists  
 156 of two major parts: (1) the Threshold Matched Precipitation Index (TMPI) algorithm,  
 157 which was used to derive precipitation estimates between 40°N-40°S from low-earth-orbit  
 158 and geostationary IR datasets, with adjustments made to PMW-derived precipitation  
 159 occurrence; and (2) the algorithm developed by Susskind et al. (1997), which was used  
 160 to estimate precipitation over latitudes beyond 40° using the TIROS Operational Ver-  
 161 tical Sounder (TOVS; before 2003) or the Advanced Infrared Sounder (AIRS; since 2003)  
 162 data. Finally, these daily precipitation estimates were calibrated to the GPCP Version  
 163 2.3 satellite-gauge monthly product to ensure accuracy and consistency (Adler et al., 2020;  
 164 Huffman, 1997).

165 The GPCP Version 3.2 (hereinafter referred to as "GPCP v3.2") aims to improve  
 166 the accuracy and resolution of precipitation estimates by utilizing the increased num-  
 167 ber of spaceborne sensors and enhanced merging algorithms in the NASA Global Pre-

168 precipitation Mission (GPM) era. GPCP v3.2 provides daily, global  $0.5^\circ$  gridded precipitation  
 169 estimates from June 2000 through September 2021 (Huffman et al., 2023a). Compared to GPCP v1.3,  
 170 the major difference in GPCP v3.2 is the replacement of TMPI  
 171 algorithm with NASA's Integrated MultisatellitE Retrievals for the GPM mission (IMERG)  
 172 algorithm (Huffman et al., 2019). IMERG Final Run precipitation estimates are used  
 173 between  $55^\circ\text{N}$ - $55^\circ\text{S}$ , while TOVS/AIRS based precipitation estimates are employed at  
 174 higher latitudes. These precipitation estimates were then calibrated to the new GPCP  
 175 v3.2 monthly product (Huffman et al., 2023b) that uses the Merged CloudSat, NASA  
 176 TRMM (Tropical Rainfall Measuring Mission), and NASA GPM climatological precip-  
 177 itation product (MCTG; Behrangi & Song, 2020) over the mid- and high-latitudes oceans  
 178 and an updated Tropical Composite Climatology (TCC; Adler et al., 2009; Wang et al.,  
 179 2014) over the tropical oceans for climatological calibration of the GPCP. In addition,  
 180 GPCP v3.2 contains a diagnostic data field, the probability of liquid phase (PLP; %),  
 181 which accompanies the precipitation estimates to inform the precipitation phase.

182 The GPCP v3.2 daily product became available in 2022 with the intention of even-  
 183 tually replacing GPCP v1.3 (Huffman et al., 2023a). While GPCP v1.3 has been widely  
 184 used and discussed in many climate-, ocean- and water-related studies (e.g., Masunaga  
 185 et al., 2019; Yu, 2019; Arabzadeh et al., 2020), the validation of GPCP v3.2 is rarely done,  
 186 especially over oceans due to its recent release and limited reference observations over  
 187 oceans. The following analyses will be conducted in a comparative manner, with a fo-  
 188 cuse on GPCP v3.2 and its relative performance compared to GPCP v1.3.

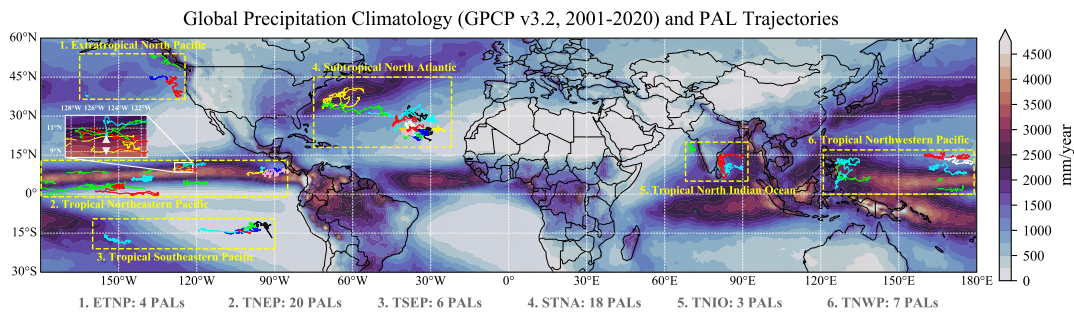


**Figure 1.** The trajectories of 58 PALs used in this study, on the global precipitation climatology map derived from GPCP v3.2 (2001-2020). Different colors are used for individual PALs to enhance visibility. The two white triangles in the zoomed-in inset show the fixed locations of PALs (on buoy moorings) that were deployed in the tropical Eastern Pacific during SPURS-2.

### 189 3 Methodology

190 The PAL data are matched to the GPCP  $1^\circ$  (v1.3) and  $0.5^\circ$  (v3.2) grids at daily  
 191 intervals. Each 1-minute PAL rain sample is assigned to a GPCP grid based on its sam-  
 192 pling location. All 1-minute PAL data samples within a given GPCP grid are then av-  
 193 eraged across the daily time window to compute the daily averaged rain rate from PAL.  
 194 This matching and averaging procedure is applied to each PAL, resulting in 58 paired  
 195 PAL-GPCP daily data series. The drifting PALs are unlikely to traverse multiple GPCP  
 196 grid boxes in a day, as Argo floats typically move less than 3 km/day when drifting at  
 197 a 1-km depth (Lebedev et al., 2007; Ollitrault & Colin de Verdière, 2014). Our eval-  
 198 uation is limited to liquid precipitation (i.e., rainfall), so the paired PAL-GPCP data with  
 199 a PLP value (from GPCP v3.2) below 100 are excluded from the subsequent analyses.  
 200 Approximately 0.8% of the total daily data samples are removed, mainly from the PALs  
 201 deployed beyond  $35^\circ\text{N}$ .

For each PAL, the paired PAL-GPCP daily data are accumulated monthly, and then the daily and monthly data are averaged through the PAL's operational period to calculate the multi-year mean monthly and daily rainfall. We compare these paired daily, monthly, and multi-year mean PAL-GPCP estimates, and evaluate the performance of GPCP in terms of rain detection and rain rate estimation. For rain detection (daily scale only), we calculate the contingency table statistics including the probability of detection (POD), false alarm ratio (FAR), and Heidke skill score (HSS) based on a rain/no-rain detection threshold of 0.5 mm/day. For rain rate estimation, we use relative bias (RB), root-mean-square error (RMSE), normalized root-mean-square error (NRMSE), and the Pearson correlation coefficient (CC). These four metrics are computed either unconditionally (using all PAL-GPCP data including zeros) or conditionally (excluding zeros; i.e., for "hits" only).

We also group the PALs into six regions based on the ocean and latitudes where they are deployed (as shown in Figure 1): (1) 4 PALs in the extratropical North Pacific (ETNP); (2) 20 PALs in the tropical Northeastern Pacific (TNEP); (3) 6 PALs in the tropical Southeastern Pacific (TSEP); (4) 18 PALs in the subtropical North Atlantic (STNA); (5) 3 PALs in the tropical North Indian Ocean (TNIO); and (6) 7 PALs in the tropical Northwestern Pacific (TNWP). The evaluation results will be summarized using this grouping to understand the region-dependent performance of GPCP.

To investigate GPCP's daily performance as a function of rainfall intensity, we calculate the evaluation metrics under various rain detection thresholds (1, 2, 4, ..., 256 mm/day). We combine all the PAL-GPCP daily data for this analysis to ensure sufficient data samples. In addition, two probability distribution functions (PDF), the precipitation occurrence PDF (PDFc) and volume PDF (PDFv) are also computed, following the method detailed in Li et al. (2013).

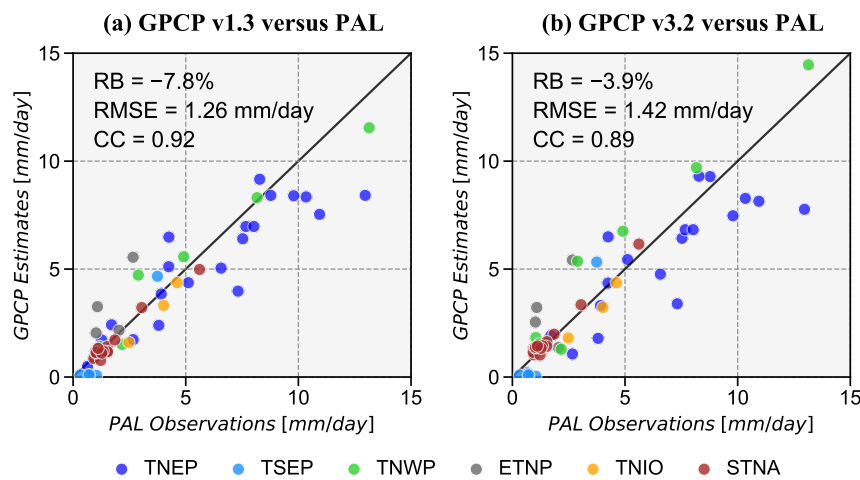


**Figure 2.** Scatterplots comparing the multi-year mean rain rates (mm/day) estimated by (a) GPCP v1.3 and (b) GPCP v3.2 against PAL observations. Each data point corresponds to one PAL, and the color indicates its group by region.

227 **4 Results**

228 **4.1 Comparison of Multi-year Mean**

229 Figure 2 compares the multi-year mean rain rates obtained from the two GPCP  
 230 products and PALs. The GPCP estimates are highly correlated with in-situ observations,  
 231 showing the reliability of GPCP products in characterizing rainfall climatology over oceans.  
 232 The difference between the two GPCP versions is generally small. While GPCP v3.2 has  
 233 slightly improved the underestimation bias compared to GPCP v1.3, it has introduced  
 234 additional variability, resulting in larger RMSE and lower CC values. This increased vari-  
 235 ability can be partially attributed to the higher spatial resolution of GPCP v3.2, which  
 236 has led to realistic sub-degree variations in precipitation estimates. Despite the overall  
 237 similarity to v1.3, GPCP v3.2 has region-dependent changes. For example, v3.2 has con-  
 238 sistently increased multi-year mean rain rates over the tropical Northwestern Pacific and  
 239 decreased multi-year mean rain rates at the tropical Northeastern Pacific. Furthermore,  
 240 the region-dependent visualization in Figure 2 highlights that both GPCP versions have  
 241 significantly underestimated rainfall over the tropical Southeastern Pacific, which will  
 242 be further discussed below.

243 **4.2 Seasonality and Monthly Evaluation**

244 GPCP v1.3 and v3.2 perform similarly in representing the seasonality and intra-  
 245 annual variations of rainfall over most regions (Figs. 3a, c, e-f), and there are no con-  
 246 sistent relative improvements in GPCP v3.2 at monthly scale. For example, GPCP v3.2  
 247 better captures the seasonality in the second half of the year over the tropical North In-  
 248 dian Ocean (Fig. 3e), but its overestimation bias at the tropical Northwestern Pacific  
 249 is further increased during the summer (Fig. 3c; also see Table S1 in the Supporting In-  
 250 formation).

251 On the other hand, the GPCP estimates significantly differ from PAL observations  
 252 in the tropical Southeastern Pacific and extratropical North Pacific, as shown in Figs.  
 253 3b and d. Specifically, the two GPCP products consistently underestimate rainfall by  
 254 about 60% (see Table S1) throughout all months in the tropical Southeastern Pacific.  
 255 This is likely due to the known limitation of PMW/IR sensors in detecting light and/or  
 256 shallow convective tropical rainfall, which results in a substantial amount of undetected  
 257 rain (Behrangi et al., 2012; Schumacher & Houze, 2003). For the high-latitude North Pa-  
 258 cific, the discrepancy between GPCP and PAL is most noticeable during winter months  
 259 (Nov.-Feb.), with GPCP estimates being considerably higher than PAL observations (rel-  
 260 ative bias exceeds 100%; see Table S1). This is likely because the filtered GPCP daily  
 261 estimates still contain a considerable amount of solid precipitation due to the imperfect  
 262 diagnostic variable PLP (Huffman et al., 2023a). The portion of liquid vs. solid is not  
 263 captured by the PALs since, to date, the PALs and associated algorithms have only been  
 264 designed for quantifying liquid rainfall (though quantifying snowfall is a future research  
 265 possibility). Nevertheless, this comparison highlights the challenge of accurately mea-  
 266 suring wintertime rainfall with GPCP.

267 **4.3 Daily Rainfall Detection and Estimation Skills**

268 Figure 4 presents the spatial maps of daily evaluation metrics for GPCP products,  
 269 with detailed statistics provided in Table S2 in the Supporting Information. Compared  
 270 to the previous version (left panels in Fig. 4), GPCP v3.2 (right panels in Fig. 4) shows  
 271 remarkable improvement at daily scale. For rainfall detection (Figs. 4a-c and g-i), it con-  
 272 sistently reduces FAR and thus increases HSS (also see Table S2). After detection, it fur-  
 273 ther improves rain rate estimation with an increased CC at most locations (Figs. 4f, l).  
 274 In addition, visual comparison of the bias maps (Figs. 4d, j) suggests that GPCP v3.2  
 275 generally overestimates rain rates while GPCP v1.3 is dominated by underestimation.

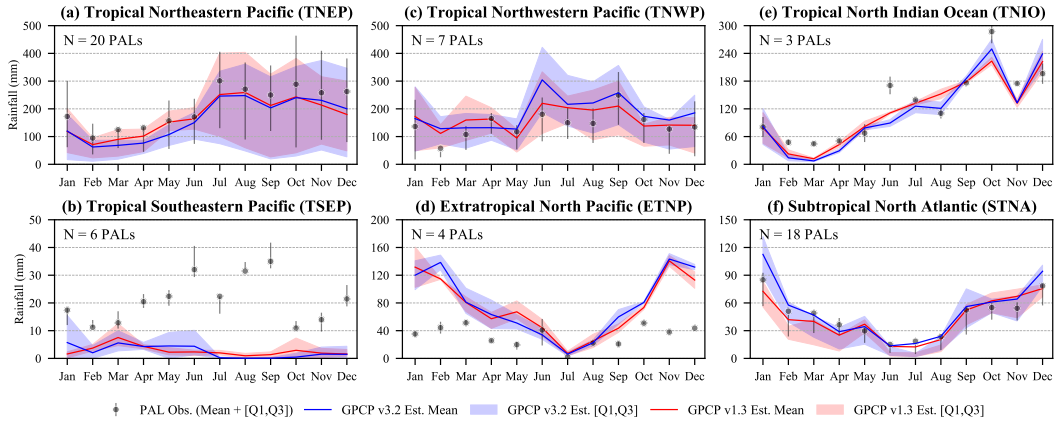


**Figure 3.** Intra-annual distributions of monthly rainfall estimated from GPCP v1.3, GPCP v3.2 and PAL over different regions (as shown in Fig 1). The comparison includes the mean, and interquartile range (IQR, i.e., the difference between 25% and 75% quantile, [Q1, Q3]) estimates of monthly rainfall, which are calculated from N PALs within each region. Here, N represents the number of PALs.

These relative changes are largely attributed to the incorporation of IMERG Final Run into GPCP v3.2. It suggests that the more direct use of PMW information through IMERG in GPCP V3.2 daily product, results in the observed improvement over GPCP v1.3 that uses TMPI algorithm instead of IMERG.

The rain detection ability of GPCP v3.2 appears to vary across different ocean regions as summarized by HSS (Fig. 4i). The product demonstrates the best detection skills over the tropical North Pacific, where it has the highest probability of detection ( $POD > 0.6$ ) and lowest false alarm rates ( $FAR < 0.4$ ). As it extends towards higher latitudes, either its POD decreases over the North Atlantic (with an IQR of 0.44-0.51; see Table S2) or FAR notably increases over the North Pacific (with an IQR of 0.60-0.62; see Table S2), resulting in degraded detection skills of GPCP v3.2 in these regions. Furthermore, GPCP v3.2 shows its lowest detection potential over the tropical Southeastern Pacific and North Indian Ocean, where it has minimal POD and HSS values.

Once rainfall is detected, GPCP v3.2 estimated daily rain rates correlate well with the PAL data (with a CC greater than 0.5; Fig. 4l) in most areas, except for the tropical Southeastern Pacific. The conditional estimation bias shows a mixed pattern with both negative and positive values in the tropical oceans, while it tends to be dominated by overestimation at higher latitudes, e.g., the North Atlantic and the North Pacific (see Fig. 4j). This overestimation bias peaks in the North Pacific, which is consistent with the monthly results as shown in Fig. 3d.

Similar to Figure 3, Figure 4 also highlights the difference of the rainfall estimates from GPCP and PAL over the tropical Southeastern Pacific and extratropical North Pacific, but with more insights. For tropical Southeastern Pacific, there appears to be more as a “detection” issue since the GPCP and PAL data are barely correlated, exhibiting both low POD and high FAR. In contrast, the extratropical North Pacific is plagued by an overestimation problem, which results in high POD and high FAR. Although the exact reason needs to be further addressed and is outside the scope of this study, this result shows the large uncertainty of precipitation measurements over the two regions.

Figure 5 further shows the improvement of GPCP v3.2 over the prior version as a function of daily rainfall intensity. The PDFs (Figs. 5a-b) indicate that the prior ver-

306 sion of GPCP has underestimated the occurrence of both light (<2 mm/day) and heavy  
 307 rainfall (>20 mm/day), and overestimated the contributions from medium rainfall (4-  
 308 16 mm/day) in terms of both rain occurrence and volume. In contrast, the PDFs of GPCP  
 309 v3.2 agree very well with those of PALs, pointing to the success of this new product in  
 310 accurately representing the full spectrum of rainfall over oceans. GPCP v3.2 shows bet-  
 311 ter rainfall detection skills across all rain intensities (Fig. 5c), especially during heavy  
 312 rainfall (note the drop of HSS for GPCP v1.3 when rain rate exceeds 8 mm/day). For  
 313 those detected (i.e., “hits” ) events, GPCP v3.2 tends to overestimate rainfall under var-  
 314 ious intensities while GPCP v1.3 tends to largely underestimate it. The correlation de-  
 315 creases with increased rain rates, but the correlation value for GPCP v3.2 is consistently  
 316 higher (better) than v1.3 by about 0.16.

## 317 5 Conclusions

318 Satellite precipitation products such as GPCP have long served as valuable sources  
 319 of oceanic precipitation information, which is critical for our understanding of the cli-  
 320 mate and weather systems, global water and energy cycles, and upper ocean processes.  
 321 Prior to this study, our knowledge of GPCP precipitation estimation performance over  
 322 oceans was limited due to insufficient in-situ observations. With recent advances in oceanic  
 323 observing technology, an increasing number of PALs have been deployed in global oceans  
 324 to collect minute-scale oceanic rainfall data with a surface sampling area similar to space-  
 325 borne sensors. These PALs, mostly drifting at 1-km depth along with Argo floats plus  
 326 a several others on subsurface moorings, cover a broad expanse of ocean areas and many  
 327 years of time, providing us with an unprecedented opportunity to validate satellite pre-  
 328 cipitation estimates over oceans. Using 58 PALS as a reference Bytheway et al. (2023)  
 329 reviewed IMERG, CMORPH, and PDIR-Now, while this study evaluates the GPCP daily  
 330 products, including the widely-used GPCP v1.3 and the newly released GPCP v3.2. Through  
 331 a suite of evaluation metrics, we compare the two GPCP products and assess their per-  
 332 formance as a function of time scale, region, and rainfall intensity. To the best of our knowl-  
 333 edge, this is the first study to validate GPCP daily products using a comprehensive in-  
 334 situ oceanic dataset of PALs.

335 GPCP v1.3 and v3.2 perform similarly at multi-year scale. Their multi-year mean  
 336 rainfall estimates are highly correlated with PAL observations (CC of ~0.9) with only  
 337 slight underestimation (7.8 % for v1.3 and 3.9% for v3.2). This demonstrates their rea-  
 338 sonable performance in characterizing rainfall climatology over oceans and a slight im-  
 339 provement at multi-year time scales from v3.2. The two versions also capture well the  
 340 seasonality and intra-annual variations of rainfall over most oceans (e.g., the tropical North-  
 341 eastern Pacific, tropical Northwestern Pacific, subtropical North Atlantic, and tropical  
 342 North Indian Ocean) with comparable performance.

343 When evaluated at daily scale, GPCP v3.2 remarkably outperforms the previous  
 344 version (v1.3) in terms of rain occurrence and rain intensity. Compared to GPCP v1.3,  
 345 GPCP v3.2 reduces FAR and thus improves HSS. It also consistently increases CC at  
 346 most locations. The conditional analysis, which evaluates GPCP’s performance as a func-  
 347 tion of rain intensity, further indicates that GPCP v3.2 consistently exhibits improved  
 348 skill at different intensities. Its estimated probability distribution functions for rainfall  
 349 occurrence and volume closely align with those from PALs, whereas GPCP v1.3 under-  
 350 estimates the occurrence of both light (<2 mm/day) and heavy rainfall (>20 mm/day)  
 351 and overestimates the contributions from medium rainfall (4-16 mm/day).

352 Our evaluation highlights two regions, the tropical Southeastern Pacific and extra-  
 353 tropical North Pacific, where both versions of GPCP products exhibit similar performance  
 354 and show noticeable differences from PAL observations at multiple time scales. Although  
 355 the precise causes require detailed analysis outside the scope of this study, the present

356 work highlights the challenges of accurately measuring precipitation with GPCP in these  
357 two regions.

358 This study provides valuable insights into the performance of GPCP daily products  
359 over oceans using in-situ observations from 58 PALs across several oceanic regions.  
360 It is important to recognize that these PALs are still limited in time and spatial coverage  
361 and do not cover the entire global ocean, especially in the southern part. The deployment  
362 of additional PALs would certainly increase the opportunity to further evaluate satellite  
363 precipitation products, which is needed to understand how best to use them  
364 and how to guide their improvements.

## 365 Open Research Section

366 GPCP v1.3 daily data can be obtained from the NOAA National Centers for En-  
367 vironmental Information (NCEI) as part of NOAA Climate Data Record (CDR) Pro-  
368 gram at <https://www.ncei.noaa.gov/data/global-precipitation-climatology-project-gpcp-daily/access/>. GPCP v3.2 daily data can be accessed from the NASA God-  
369 dard Earth Sciences Data and Information Services Center (GES DISC) at [https://disc.gsfc.nasa.gov/datasets/GPCPDAY\\_3.2/summary](https://disc.gsfc.nasa.gov/datasets/GPCPDAY_3.2/summary). The PAL dataset archive is cur-  
370 rently available at <https://downloads.psl.noaa.gov/psd3/cruises/PAL/>, and will  
371 be also available at NASA ERATHDATA portal at [https://doi.org/10.5067/GPMGV-  
372 PAL/DATA101](https://doi.org/10.5067/GPMGV-PAL/DATA101).  
373

## 375 Acknowledgments

376 ZL, EJT and HC were supported in part by the National Aeronautics and Space Admin-  
377 istration (NASA) Precipitation Measurement Mission (PMM) through interagency NOAA/NASA  
378 agreement 80HQTR20T0049, in part by the NASA Ocean Salinity Science Team (OSST)  
379 through interagency NOAA/NASA agreement 80HQTR20T0046, and in part by the Na-  
380 tional Oceanic and Atmospheric Administration (NOAA) Joint Polar Satellite System  
381 (JPSS) Proving Ground and Risk Reduction (PGRR) Program. Funding went to the Co-  
382 operative Institute for Research in the Atmosphere (CIRA) at Colorado State Univer-  
383 sity through NOAA grant NA19OAR4320073. AB was supported by NASA MEaSURES  
384 (NNH17ZDA001N-MEASURES) program.

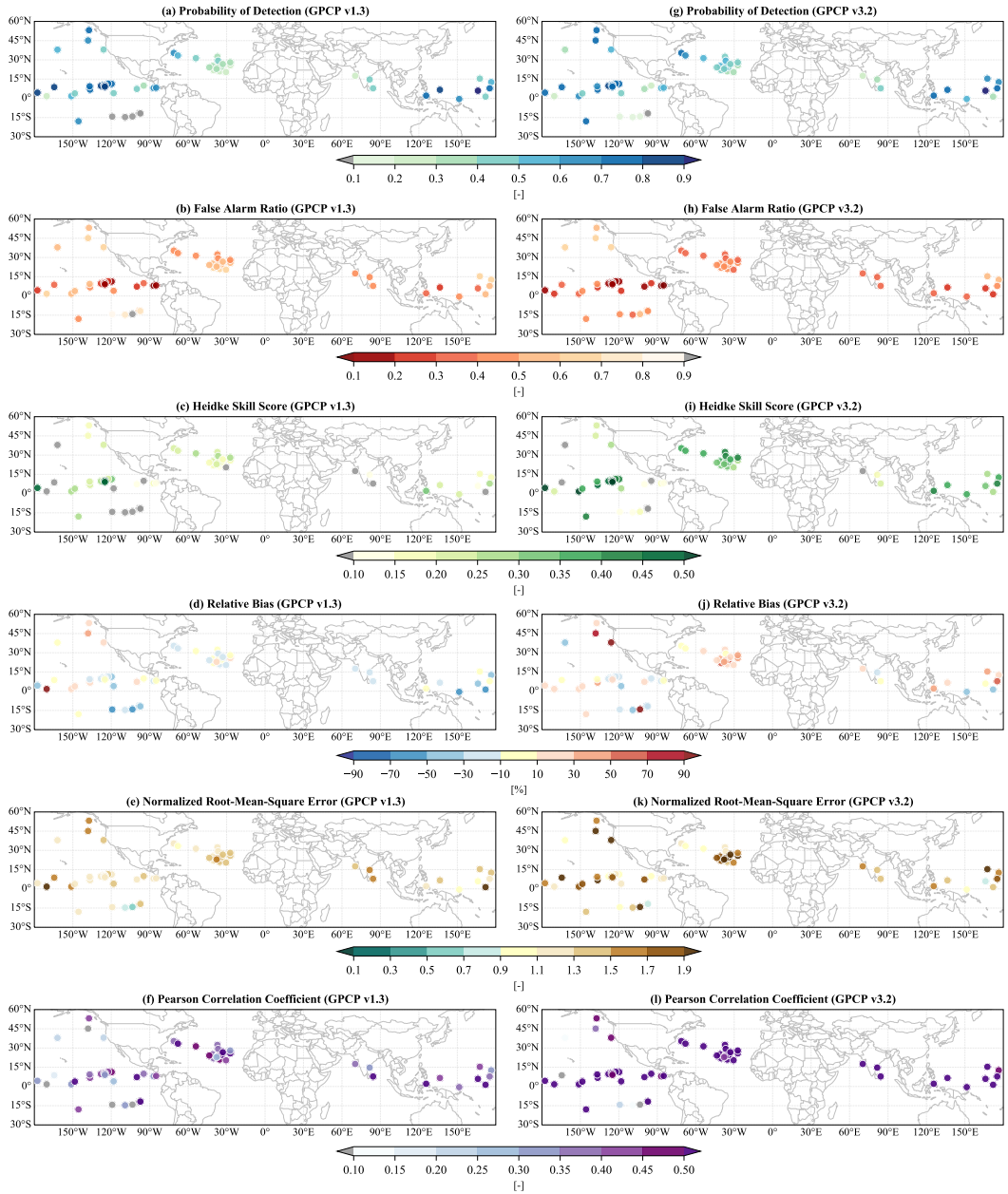


**Figure 4.** Spatial maps of (a, g) probability of detection (POD), (b, h) false alarm ratio (FAR), (c, i) Heidke skill score (HSS); and conditional (d, j) relative bias (RB), (e, k) normalized root-mean-square error (NRMSE), and (f, l) Pearson's correlation coefficient (CC) for daily GPCP v1.3 (left panels) and GPCP v3.2 (right panels) estimates against PALs. The circles represent the drifting end location of PALs, and rain detection threshold is 0.5 mm/day.

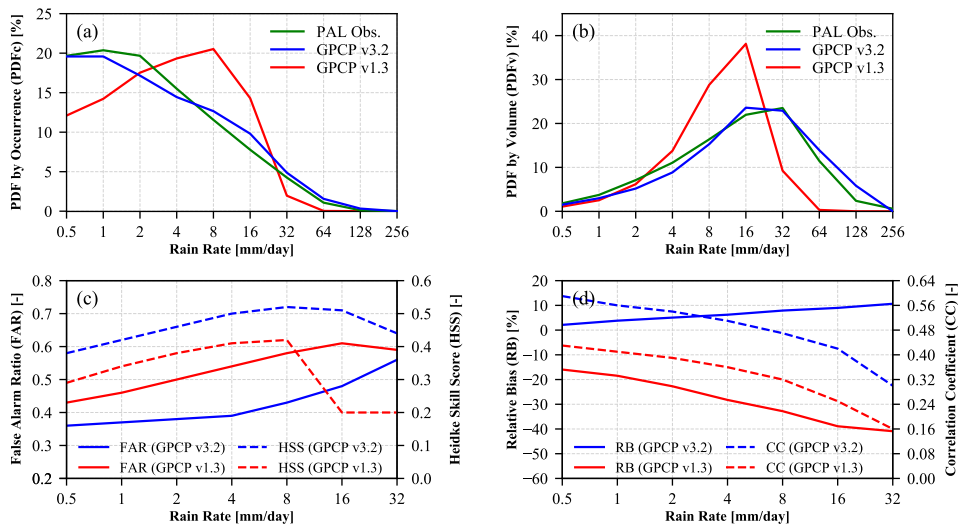


**Figure 5.** Comparison of (a) probability distribution function by occurrence (PDFc), (b) probability distribution function by volume (PDFv), (c) rainfall detection skills (FAR and HSS), and (d) estimation metrics (RB and CC) as a function of daily rainfall intensity for GPCP products.

385 **References**

- 386 Adler, R. F., Gu, G., Huffman, G. J., Sapiano, M. R. P., & Wang, J.-J. (2020).  
 387 GPCP and the Global Characteristics of Precipitation. In V. Levizzani,  
 388 C. Kidd, D. B. Kirschbaum, C. D. Kummerow, K. Nakamura, & F. J. Turk  
 389 (Eds.), *Satellite Precipitation Measurement: Volume 2* (pp. 677–697). Springer  
 390 International Publishing. doi: 10.1007/978-3-030-35798-6\_11
- 391 Adler, R. F., Huffman, G. J., Chang, A., Ferraro, R., Xie, P.-P., Janowiak, J., ...  
 392 Nelkin, E. (2003). The Version-2 Global Precipitation Climatology Project  
 393 (GPCP) Monthly Precipitation Analysis (1979–Present). *Journal of Hy-  
 394 drometeorology*, 4(6), 1147–1167. doi: 10.1175/1525-7541(2003)004<1147:  
 395 TVGPCP>2.0.CO;2
- 396 Adler, R. F., Sapiano, M., & Wang, J.-j. (2017, August). *Climate Algorithm Theo-  
 397 retical Basis Document (C-ATBD) for Global Precipitation Climatology Project  
 398 (GPCP) Daily Analysis Precipitation –GPCP Daily CDR*.
- 399 Adler, R. F., Wang, J.-J., Gu, G., & Huffman, G. J. (2009). A Ten-Year Tropical  
 400 Rainfall Climatology Based on a Composite of TRMM Products. *Journal of  
 401 the Meteorological Society of Japan. Ser. II*, 87A, 281–293. doi: 10.2151/jmsj  
 402 .87A.281
- 403 Arabzadeh, A., Ehsani, M. R., Guan, B., Hefflin, S., & Behrangi, A. (2020). Global  
 404 Intercomparison of Atmospheric Rivers Precipitation in Remote Sensing and  
 405 Reanalysis Products. *Journal of Geophysical Research: Atmospheres*, 125(21).  
 406 doi: 10.1029/2020JD033021
- 407 Arkin, P. A., & Xie, P. (1994). The Global Precipitation Climatology Project: First  
 408 Algorithm Intercomparison Project. *Bulletin of the American Meteorological  
 409 Society*, 75(3), 401–419. doi: 10.1175/1520-0477(1994)075<0401:TGCPF>2.0  
 410 .CO;2
- 411 Behrangi, A., Lebsack, M., Wong, S., & Lambrightsen, B. (2012). On the Quantifica-  
 412 tion of Oceanic Rainfall Using Spaceborne Sensors. *Journal of Geophysical Re-  
 413 search: Atmospheres*, 117(D20). doi: 10.1029/2012JD017979
- 414 Behrangi, A., & Song, Y. (2020). A New Estimate for Oceanic Precipitation Amount  
 415 and Distribution Using Complementary Precipitation Observations from Space  
 416 and Comparison with GPCP. *Environmental Research Letters*, 15(12), 124042.  
 417 doi: 10.1088/1748-9326/abc6d1
- 418 Bolvin, D. T., Huffman, G. J., Nelkin, E. J., & Tan, J. (2021). Comparison of  
 419 Monthly IMERG Precipitation Estimates with PACRAIN Atoll Observations.  
 420 *Journal of Hydrometeorology*. doi: 10.1175/JHM-D-20-0202.1
- 421 Bowman, K. P. (2005). Comparison of TRMM Precipitation Retrievals with Rain  
 422 Gauge Data from Ocean Buoys. *Journal of Climate*, 18(1), 178–190. doi: 10  
 423 .1175/JCLI3259.1
- 424 Bytheway, J. L., Thompson, E. J., Yang, J., & Chen, H. (2023). Evaluat-  
 425 ing Satellite Precipitation Estimates Over Oceans Using Passive Aquatic  
 426 Listeners. *Geophysical Research Letters*, 50(6), e2022GL102087. doi:  
 427 <https://doi.org/10.1029/2022GL102087>
- 428 Durack, P. (2015). Ocean Salinity and the Global Water Cycle. *Oceanography*,  
 429 28(1), 20–31. doi: 10.5670/oceanog.2015.03
- 430 Hartmann, D. L. (2016). Chapter 5 - The Hydrologic Cycle. In D. L. Hart-  
 431 mann (Ed.), *Global Physical Climatology (Second Edition)* (Second Edi-  
 432 tion ed., p. 131–157). Boston: Elsevier. doi: <https://doi.org/10.1016/B978-0-12-328531-7.00005-0>
- 433 Huffman, G. J. (1997). Estimates of Root-Mean-Square Random Error for Finite  
 434 Samples of Estimated Precipitation. *Journal of Applied Meteorology*, 36(9),  
 435 1191–1201. doi: 10.1175/1520-0450(1997)036<1191:EORMSR>2.0.CO;2
- 436 Huffman, G. J., Adler, R. F., Arkin, P., Chang, A., Ferraro, R., Gruber, A., ...  
 437 Schneider, U. (1997). The Global Precipitation Climatology Project (GPCP)

- 439                         Combined Precipitation Dataset. *Bulletin of the American Meteorological Society*, 78(1), 5–20. doi: 10.1175/1520-0477(1997)078<0005:TGPCPG>2.0.CO;2
- 440                         Huffman, G. J., Adler, R. F., Morrissey, M. M., Bolvin, D. T., Curtis, S., Joyce, R.,  
441                         ... Susskind, J. (2001). Global Precipitation at One-Degree Daily Resolution  
442                         from Multisatellite Observations. *Journal of Hydrometeorology*, 2(1), 36–50.  
443                         doi: 10.1175/1525-7541(2001)002<0036:GPAODD>2.0.CO;2
- 444                         Huffman, G. J., Alder, R. F., Behrangi, A., Bolvin, D. T., Nelkin, E. J., & Ehsani,  
445                         M. R. (2023a, January). *Algorithm Theoretical Basis Document (ATBD) for,*  
446                         *Global Precipitation Climatology Project Version 3.2 Daily Precipitation Data.*
- 447                         Huffman, G. J., Alder, R. F., Behrangi, A., Bolvin, D. T., Nelkin, E. J., & Ehsani,  
448                         M. R. (2023b, January). *Algorithm Theoretical Basis Document (ATBD) for,*  
449                         *Global Precipitation Climatology Project Version 3.2 Monthly Precipitation*  
450                         *Data.*
- 451                         Huffman, G. J., Bolvin, D. T., Braithwaite, D., Hsu, K., Joyce, R., Kidd, C., ...  
452                         Xie, P. (2019, March). *Algorithm Theoretical Basis Document (ATBD) Version*  
453                         *06, NASA Global Precipitation Measurement (GPM) Integrated Multi-satellite*  
454                         *Retrievals for GPM (IMERG).*
- 455                         Kidd, C., Becker, A., Huffman, G. J., Muller, C. L., Joe, P., Skofronick-Jackson, G.,  
456                         & Kirschbaum, D. B. (2017). So, How Much of the Earth's Surface Is Cov-  
457                         ered by Rain Gauges? *Bulletin of the American Meteorological Society*, 98(1),  
458                         69–78. doi: 10.1175/BAMS-D-14-00283.1
- 459                         Kidd, C., Huffman, G., Maggioni, V., Chambon, P., & Oki, R. (2021). The Global  
460                         Satellite Precipitation Constellation: Current Status and Future Requirements.  
461                         *Bulletin of the American Meteorological Society*, 102(10), E1844–E1861. doi:  
462                         10.1175/BAMS-D-20-0299.1
- 463                         Klepp, C., Michel, S., Protat, A., Burdanowitz, J., Albern, N., Kähnert, M., ...  
464                         Buehler, S. A. (2018). Oceanrain, A New In-situ Shipboard Global Ocean  
465                         Surface-reference Dataset of All Water Cycle Components. *Scientific Data*,  
466                         5(1), 1–22.
- 467                         Lagerloef, G., Schmitt, R., Schanze, J., & Kao, H.-Y. (2010). The Ocean and the  
468                         Global Water Cycle. *Oceanography*, 23(4), 82–93. doi: 10.5670/oceanog.2010  
469                         .07
- 470                         Lebedev, K., Yoshinari, H., Maximenko, N., & Hacker, P. (2007). *YoMaHa'07: Ve-*  
471                         *locity Data Assessed from Trajectories of Argo Floats at Parking Level and at*  
472                         *the Sea Surface* (Tech. Rep. No. 4(2)). IPRC Technical Note.
- 473                         Levizzani, V., Kidd, C., Aonashi, K., Bennartz, R., Ferraro, R. R., Huffman, G. J.,  
474                         ... Wang, N. (2018). The Activities of the International Precipitation Working  
475                         Group. *Quarterly Journal of the Royal Meteorological Society*, 144(S1), 3–15.  
476                         doi: 10.1002/qj.3214
- 477                         Li, Z., Yang, D., & Hong, Y. (2013). Multi-scale Evaluation of High-resolution  
478                         Multi-sensor Blended Global Precipitation Products over the Yangtze River.  
479                         *Journal of Hydrology*, 500, 157–169. doi: 10.1016/j.jhydrol.2013.07.023
- 480                         Lindstrom, E., Bryan, F., & Schmitt, R. (2015). SPURS: Salinity Processes in the  
481                         Upper-ocean Regional Study. *Oceanography*, 28(1), 14–19.
- 482                         Lindstrom, E. J., Edson, J. B., Schanze, J. J., & Shcherbina, A. Y. (2019). SPURS-  
483                         2: Salinity Processes in the Upper-Ocean Regional Study 2 – The Eastern  
484                         Equatorial Pacific Experiment. *Oceanography*, 6. doi: [https://doi.org/10.5670/](https://doi.org/10.5670/oceanog.2019.207)  
485                         oceanog.2019.207
- 486                         Ma, B. B. (2022). Rainfall at Sea: Using the Underwater Sounds of Raindrops as  
487                         a Rain Gauge for Weather and Climate. *Acoustics Today*, 18(2), 62. doi: 10  
488                         .1121/AT.2022.18.2.62
- 489                         Ma, B. B., & Nystuen, J. A. (2005). Passive Acoustic Detection and Measurement of  
490                         Rainfall at Sea. *Journal of Atmospheric and Oceanic Technology*, 22.
- 491                         Masunaga, H., Schröder, M., Furuzawa, F. A., Kummerow, C., Rustemeier,  
492                         E., & Schneider, U. (2019). Inter-product Biases in Global Precipita-

- tion Extremes. *Environmental Research Letters*, 14(12), 125016. doi: 10.1088/1748-9326/ab5da9
- Moum, J., & Smyth, W. (2019). Upper Ocean Mixing. In *Encyclopedia of Ocean Sciences* (pp. 71–79). Elsevier. doi: 10.1016/B978-0-12-409548-9.11573-8
- Nystuen, J., Riser, S., Wen, T., & Swift, D. (2011). Interpreted Acoustic Ocean Observations from Argo Floats. *The Journal of the Acoustical Society of America*, 129(4), 2400–2400. doi: 10.1121/1.3587814
- Nystuen, J. A., Anagnostou, M. N., Anagnostou, E. N., & Papadopoulos, A. (2015). Monitoring Greek Seas Using Passive Underwater Acoustics. *Journal of Atmospheric and Oceanic Technology*, 32(2), 334–349. doi: 10.1175/JTECH-D-13-00264.1
- O’Kane, T. J., Monselesan, D. P., & Maes, C. (2016). On the Stability and Spatiotemporal Variance Distribution of Salinity in the Upper Ocean. *Journal of Geophysical Research: Oceans*, 121(6), 4128–4148. doi: 10.1002/2015JC011523
- Ollitrault, M., & Colin de Verdier, A. (2014). The Ocean General Circulation near 1000-m Depth. *Journal of Physical Oceanography*, 44(1), 384–409. doi: 10.1175/JPO-D-13-030.1
- Pfeifroth, U., Mueller, R., & Ahrens, B. (2013). Evaluation of Satellite-Based and Reanalysis Precipitation Data in the Tropical Pacific. *Journal of Applied Meteorology and Climatology*, 52(3), 634–644. doi: 10.1175/JAMC-D-12-049.1
- Riser, S., Yang, J., & Drucker, R. (2019). Observations of Large-Scale Rainfall, Wind, and Sea Surface Salinity Variability in the Eastern Tropical Pacific. *Oceanography*, 32(2), 42–49. doi: 10.5670/oceanog.2019.211
- Roemmich, D., Alford, M. H., Claustre, H., Johnson, K., King, B., Moum, J., ... Yasuda, I. (2019). On the Future of Argo: A Global, Full-Depth, Multi-Disciplinary Array. *Frontiers in Marine Science*, 6, 439. doi: 10.3389/fmars.2019.00439
- Rutledge, S., Chandrasekar, V., Fuchs, B., George, J., Junyent, F., Kennedy, P., & Dolan, B. (2019). Deployment of the SEA-POL C-band Polarimetric Radar to SPURS-2. *Oceanography*, 32(2), 50–57. doi: 10.5670/oceanog.2019.212
- Sallée, J.-B., Pellichero, V., Akhoudas, C., Pauthenet, E., Vignes, L., Schmidtko, S., ... Kuusela, M. (2021). Summertime increases in upper-ocean stratification and mixed-layer depth. *Nature*, 591(7851), 592–598. doi: 10.1038/s41586-021-03303-x
- Sapiro, M. R. P., & Arkin, P. A. (2009). An Intercomparison and Validation of High-Resolution Satellite Precipitation Estimates with 3-Hourly Gauge Data. *Journal of Hydrometeorology*, 10(1), 149–166. doi: 10.1175/2008JHM1052.1
- Schmitt, R. W. (1995). The Ocean Component of the Global Water Cycle. *Reviews of Geophysics*, 33(S2), 1395–1409. doi: 10.1029/95RG00184
- Schumacher, C., & Houze, R. A. (2003). The TRMM Precipitation Radar’s View of Shallow, Isolated Rain. *Journal of Applied Meteorology*, 42(10), 1519–1524. doi: 10.1175/1520-0450(2003)042<1519:TTPRVO>2.0.CO;2
- Smith, N., Kessler, W. S., Cravatte, S., Sprintall, J., Wijffels, S., Cronin, M. F., ... Brunner, S. (2019). Tropical Pacific Observing System. *Frontiers in Marine Science*, 6, 31. doi: 10.3389/fmars.2019.00031
- Susskind, J., Piraino, P., Rokke, L., Iredell, L., & Mehta, A. (1997). Characteristics of the TOVS Pathfinder Path A Dataset. *Bulletin of the American Meteorological Society*, 78(7), 1449–1472. doi: 10.1175/1520-0477(1997)078<1449:COTTPP>2.0.CO;2
- Trenberth, K. E., Smith, L., Qian, T., Dai, A., & Fasullo, J. (2007). Estimates of the Global Water Budget and Its Annual Cycle Using Observational and Model Data. *Journal of Hydrometeorology*, 8(4), 758–769. doi: 10.1175/JHM600.1
- Wang, J.-J., Adler, R. F., Huffman, G. J., & Bolvin, D. (2014). An Updated TRMM

- 549           Composite Climatology of Tropical Rainfall and Its Validation. *Journal of Climate*, 27(1), 273–284. doi: 10.1175/JCLI-D-13-00331.1
- 550
- 551           Yang, J., Nystuen, J. A., Riser, S. C., & Thorsos, E. I. (2023). Open Ocean Ambient
- 552           Noise Data in the Frequency Band of 100 Hz–50 kHz from the Pacific Ocean.
- 553           *JASA Express Letters*, 3(3), 036001. doi: 10.1121/10.0017349
- 554           Yang, J., Riser, S., Nystuen, J., Asher, W., & Jessup, A. (2015). Regional Rainfall
- 555           Measurements Using the Passive Aquatic Listener During the SPURS Field
- 556           Campaign. *Oceanography*, 28(1), 124–133. doi: 10.5670/oceanog.2015.10
- 557           Yu, L. (2011). A Global Relationship Between the Ocean Water Cycle and Near-
- 558           surface Salinity. *Journal of Geophysical Research: Oceans*, 116(C10). doi:
- 559           <https://doi.org/10.1029/2010JC006937>
- 560           Yu, L. (2019). Global Air–Sea Fluxes of Heat, Fresh Water, and Momentum: Energy
- 561           Budget Closure and Unanswered Questions. *Annual Review of Marine Science*,
- 562           11(1), 227–248. doi: 10.1146/annurev-marine-010816-060704